JEECS (Journal of Electrical Engineering and Computer Sciences)
Vol. 11, No. 1, June 2026, pp. 67-76
e-ISSN: 2579-5392 p-ISSN: 2528-0260

Harmonic Performance in Hybrid AC-DC Microgrid Connected Bidirectional Converter with LCL Filter

Hasti Afianti, Ahmadi, Saidah, Richa Watiasih, Bambang Purwahyudi

Department of Electrical Engineering, Faculty of Engineering, Universitas Bhayangkara Surabaya, Jl. Ahmad Yani 114, Surabaya, 60231, Indonesia

Article Info

Article history:
Received: 25 February 2026
Revised: 2 May 2026
Accepted: 18 May 2026

Keyword:
AC-DC microgrid
Bidirectional converter
Grid connected inverter
Hybrid
LCL filter

Abstract

This paper presents the harmonic performance of a grid-connected hybrid AC-DC microgrid. Using solar power as a source in the DC microgrid and the grid in the AC microgrid eliminates the need for energy storage. Solar power generation is known to be intermittent, requiring a power supply to meet the load demand in the DC microgrid. Therefore, a converter that can operate as both an inverter and a rectifier is required. One way to address this issue is to use a bidirectional AC-DC converter (BC). To perform its function, this converter requires a filter to reduce the switching frequency ripple current injected into the grid. Among the available options, the LCL filter is widely recognized as the most effective solution for suppressing switching frequency harmonics. In this study, the performance of the LCL filter will be analyzed through simulations using MATLAB/Simulink. The results show that the bidirectional AC-DC converter designed with the LCL filter effectively suppresses resonances occurring at the converter output in rectifier or inverter mode., the voltage in the AC microgrid remained stable, the THD stayed below 5%, and the system frequency was well maintained. However, during the standby period, when the power transfer in both the DC and AC microgrids is zero, the THD on the grid remains high, up to 200%.

Corresponding author:
Hasti Afianti, hasti_afianti@ubhara.ac.id

DOI: https://doi.org/10.54732/jeecs.v11i1.7

1. Introduction

Lasseter with his new electricity concept, distribution generators that supply the surrounding load into a subsystem or microgrid of the distribution system makes the starting point of change in the conventional electricity [1]. Research on microgrid has been growing, AC microgrids, DC microgrids, and combination of them was known as hybrid AC-DC microgrids [2], [3]. On an AC microgrid, there are main buses that use the AC system, as well as on DC microgrids, where the main bus uses the DC system. In both types of microgrid, both source and load will use the system on the main bus type is described in many researchs [4], [5], [6].

A hybrid AC-DC microgrid system is the combination of the two. There are two central buses, DC bus and AC bus, and they are connected with an interlinking converter as illustrated in Figure 1. The interlinking converter has a very important role. This power electronics equipment is expected to be able to flow power from an AC microgrid to a DC microgrid if the power generated by a DC source cannot supply the load power requirements. Conversely, if a DC source produces excess power from the DC load requirements, this converter must be able to transfer this excess power to the AC microgrid to be traded. That is way better use AC-DC bidirectional converter for an interlinking converter. Even now, many microgrid systems with DER do not use batteries or storage systems [7], [8]. Power delivered by these converters must be of high quality [9]. However, the switching actions of semiconductor devices introduce harmonics into the voltage and current waveforms, which are very dangerous for electric power system equipment and must be prevented from entering the network [10], [11].

The most effective filter for suppressing of the current harmonics occurring from the switching frequency injected into the grid is the LCL filter, than L filter [12]. The LCL filter must be designed appropriately to achieve high quality grid currents. More specifically, the inverter-side inductor plays a key role in reducing the maximum ripple of the inverter output current. In general, the maximum current ripple decreases as the value of inverter-side inductor increases. However, increasing inverter-side inductor also makes the filter bulkier and more expensive. Therefore, a reasonable compromise must be reached between the selected value of inverter-side inductor and the allowable current ripple [13], [14].

The capacitor(s) in the middle branch of the LCL filter provide a low-impedance path for high-frequency ripple currents and help prevent switching harmonics from propagating into the grid. To limit reactive power injection and avoid resonance issues, it is commonly recommended that the capacitor size in LCL filters should not exceed approximately 5% of the system's nominal capacitance [15], [16]. Comprehensive investigation of the LCL filter component values using conventional mathematical theory can actually increase the stability and THD values of current and voltage [17]. Using ANN-based MPPT replaces conventional "trial-and-error" algorithms like Perturb and Observe (P&O), significantly reducing voltage ripples and switching-induced noise that contribute to harmonic distortion in grid-tied PV systems, 3-5% THD reduction is typical in optimized designs [18]. The Crown Porcupine Optimization (CPO) algorithm improves steady-state stability in microgrids by automating the tuning of control parameters to reduce non-linear distortions, thereby reducing THD from double digits to below 4% [19].

In this paper, the LCL filter in an AC-DC bidirectional converter connected to hybrid AC-DC microgrids was built by Simulink / Matlab. The built system is connected to a grid without a storage system. The simulation is carried out by providing power and load changes to prove the control performance compact the LCL filter of the bidirectional converter working properly. The power changes occur, followed by changes in load. Section II described the system configuration with the bidirectional converter, followed by the simulation and discussion in Section III. This section discusses the converter in the standby mode, which has never been done in another paper, and the conclusion in Section IV.

2. Research Methodology

2.1. Power Flow in Hybrid AC-DC Microgrid

This system is composed of three major components: the DC microgrid, the AC microgrid, and the bidirectional AC-DC converter as an interlinking converter, as presented in Figure 1. The DC microgrid includes DC sources—such as photovoltaic (PV) panels and fuel cells—that supply power to DC loads. Meanwhile, the hybrid AC–DC microgrid is connected to the main utility grid, which serves as the AC power source. The main grid is expected to provide both real (active) and reactive power to the network, supporting operation on both the AC microgrid side and the DC microgrid through the interlinking converter. In this configuration, the grid not only helps maintain overall power balance but also contributes to system stability. Specifically, the grid's active and reactive power support voltage and frequency regulation throughout the entire hybrid AC-DC microgrid [20], [21].

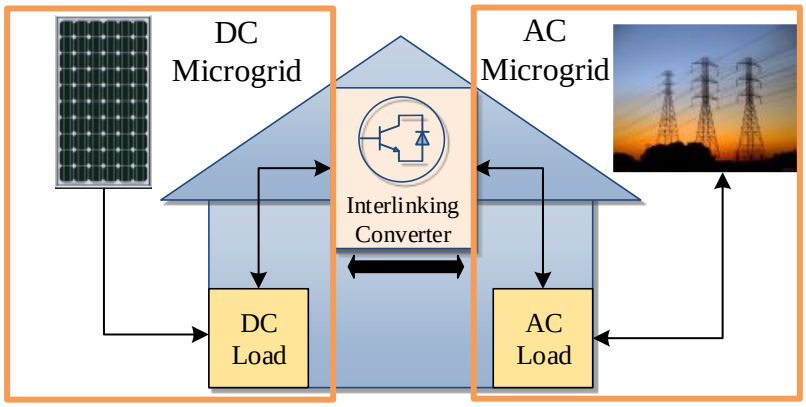

Figure 1. Power flow in hybrid AC-DC microgrid

Case 1. $\sum P_{DCSource} > \sum P_{DCLoad}$

Whare $\sum P_{DCSource}$ is the combined power generated including solar PV and battery (discharge), and $\sum P_{DCLoad}$ is the total power of the DC load and battery in charging state. In this case, the DC microgrid power generation $\sum P_{DCSource}$ exceeds load consumption. The exceed power flows to the AC sub grid through BC, which can be calculated as.

$$P_{BC} = \sum P_{DCSource} - \sum P_{DCLoad} - \sum P_{DCLoss} \quad (1)$$

Whare $\sum P_{DCLoss}$ represents the power loss induced by DC/DC converter and line impedance. In this situation The BC is in inverter mode.

Case 2. $\sum P_{DCSource} < \sum P_{DCLoad}$

Power flow from AC to DC microgrid through BC occurs, as the residual power induced by the difference between $\sum P_{DCSource}$ and DC load power consumption is negative, $P_{BC} < 0$. In this situation The BC is in rectivier mode.

Case 3. $\sum P_{DCSource} = \sum P_{DCLoad}$

The power is balanced in the DC microgrid and there is no power flow between AC and DC microgrid. Hence, $P_{BC} = 0$. In grid-tied state, AC bus voltage/frequency is controlled by utility grid (UG). BC power flow is determined by the power balance in DC microgrid. The BC is in standby mode without active power transmission [22].

2.2 AC-DC Bidirectional Converter With LCL Filter

The interlinking converter connects the DC microgrid with the AC microgrid. It is implemented using a six-switch (six-IGBT) bridge configuration, as illustrated in Figure 2. The converter receives control inputs from both sides: on the AC side, the controller uses measured grid current and voltage, while on the DC side it uses the DC bus voltage. By utilizing feedback from both microgrids, the converter can operate bidirectionally functioning either as a rectifier or as an inverter. This allows it to convert DC power to AC power or AC power to DC power, depending on the instantaneous power requirements and availability on each side of the hybrid microgrid.

Figure 2 illustrates the topology of AC-C bidirectional converter equipped with LCL filter. The load voltage is denoted as u_{dc} , while v_{dc} represents the DC voltage source used to enable bidirectional power flow. $Z_{ac\ Load}$ consist of a resistor and an inductor as a load in AC sub- microgrid [23].

The filter network consists of $L_1 - C_f - L_2$ forming an LCL structure. It is well established that, in the low-frequency range, an LCL filter behaves similarly to a single-inductor filter [24]. Where the equivalent inductance and resistance are $L = L_1 + L_2 + L_{ac\ Load}$ and $R = R_1 + R_2 + R_{ac\ Load}$. Therefore, the low-frequency mathematical model of the LCL filter can be obtained by neglecting the filter capacitor C_f [25].

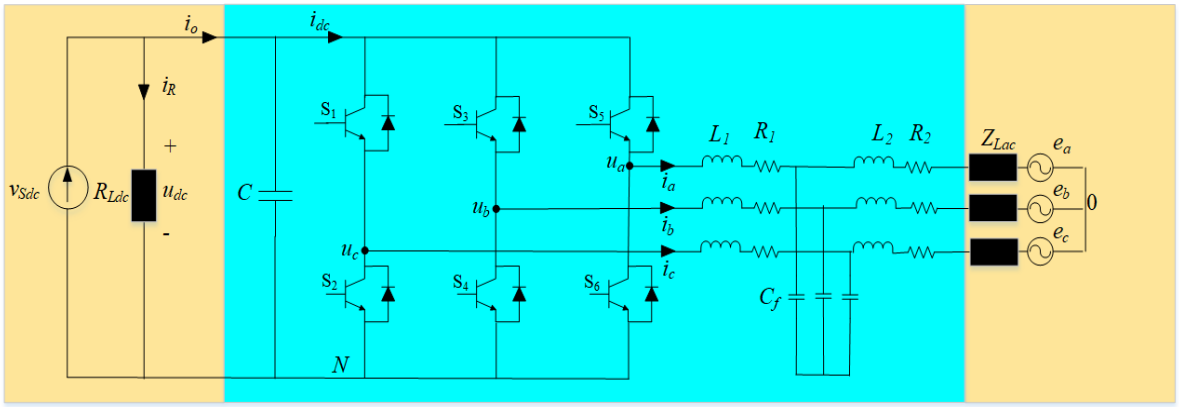

Figure 2. Hybrid AC-DC microgrid with bidirectional converter circuit

Rectifier Mode

In rectifier operation, the AC source delivers power through the converter to the DC side. Using the low-frequency approximation of the LCL filter. Whare the e_x is grid voltage source, and i_x is the phase current [26]:

$$e_x = E_m \cos(\omega t - \frac{2\pi k}{3}) \tag{2}$$

$$i_x = I_m \cos(\omega t - \frac{2\pi k}{3}) \tag{3}$$

Where k = 0, 1, 2 and x = a, b, c respectively, and ω is the grid frequency in rad/s. The per-phase equivalent circuit is given as:

$$L\frac{di_x}{dt} + Ri_x = e_x - u_x = e_x - (u_{xN} + u_{N0}) \tag{4}$$

The converter side phase to neutral voltage u_{xN} and the neutral to ground voltage u_{N0} can be expressed as follows:

$$u_{xN} = u_{dc} S_x \tag{5}$$

$$u_{N0} = -\frac{u_{dc}}{3} \sum_{x=a,b,c} S_x \tag{6}$$

Where S_x is the switching function.

$$S_x = \begin{cases} 1, S_x \ odd \ is \ on \ and \ S_x \ even \ is \ off \\ 0, S_x \ even \ is \ on \ and \ S_x \ odd \ is \ off \end{cases} \tag{7}$$

By substituting Equations (5), and (6) into equation (4), one can obtain:

$$L\frac{di_x}{dt} + Ri_x = e_x - u_x = e_x - u_{dc}\left(S_x - \frac{1}{3}\sum_{x=a,b,c} S_x\right) \tag{8}$$

The DC current can be expressed as a function of three phase current:

$$i_{dc} = S_a i_a + S_b i_b + S_c i_c \tag{9}$$

A group of differential equations can be formulated in matrix form as shown in Equation (10):

$$L\begin{bmatrix} \frac{di_a}{dt} \\ \frac{di_b}{dt} \\ \frac{di_c}{dt} \end{bmatrix} + R\begin{bmatrix} i_a \\ i_b \\ i_c \end{bmatrix} = \begin{bmatrix} e_a \\ e_b \\ e_c \end{bmatrix} - u_{dc}\begin{bmatrix} S_a - \frac{1}{3}\sum_{x=a,b,c} S_x \\ S_b - \frac{1}{3}\sum_{x=a,b,c} S_x \\ S_c - \frac{1}{3}\sum_{x=a,b,c} S_x \end{bmatrix} \tag{10}$$

$$C\frac{du_{dc}}{dt} = [S_a \quad S_a \quad S_a]\begin{bmatrix} i_a \\ i_b \\ i_c \end{bmatrix} - \frac{u_{dc}}{R_{Ldc}} - i_{Ldc} \tag{11}$$

For control design, the three-phase variables in the stationary abc frame are transformed into the synchronous rotating dq frame using the Park transformation. Applying this transformation to the per-phase loop equation, equation 4 becomes:

$$L\begin{bmatrix} \frac{di_d}{dt} \\ \frac{di_q}{dt} \end{bmatrix} + R\begin{bmatrix} i_d \\ i_q \end{bmatrix} = \begin{bmatrix} e_d \\ e_q \end{bmatrix} + \begin{bmatrix} 0 & \omega L \\ -\omega L & 0 \end{bmatrix}\begin{bmatrix} i_d \\ i_q \end{bmatrix} - \begin{bmatrix} S_d \\ S_q \end{bmatrix} u_{dc} \tag{12}$$

$$C\frac{du_{dc}}{dt} = \frac{3}{2}[S_d \quad S_q]\begin{bmatrix} i_d \\ i_q \end{bmatrix} - \frac{u_{dc}}{R_{Ldc}} - i_{Ldc} \tag{13}$$

Where e_{dq} is the magnitude of the source voltage vector

Inverter Mode

In inverter operation, the DC source delivers power to the converter, and the energy flows from the DC side back to the AC side. Although the direction of power reverses, the electrical path and filter dynamics remain the same; therefore, the differential equation is obtained by reversing the relative polarity between the converter voltage and the grid voltage in the per-phase loop.

Thus, the per-phase dynamic equation in inverter mode becomes:

$$L\begin{bmatrix} \frac{di_a}{dt} \\ \frac{di_b}{dt} \\ \frac{di_c}{dt} \end{bmatrix} + R\begin{bmatrix} i_a \\ i_b \\ i_c \end{bmatrix} = u_{dc}\begin{bmatrix} S_a - \frac{1}{3}\sum_{x=a,b,c} S_x \\ S_b - \frac{1}{3}\sum_{x=a,b,c} S_x \\ S_c - \frac{1}{3}\sum_{x=a,b,c} S_x \end{bmatrix} - \begin{bmatrix} e_a \\ e_b \\ e_c \end{bmatrix} \tag{14}$$

$$C\frac{du_{dc}}{dt} = -[S_a \quad S_a \quad S_a]\begin{bmatrix} i_a \\ i_b \\ i_c \end{bmatrix} - \frac{u_{dc}}{R_{Ldc}} + i_{Ldc} \tag{15}$$

Using the Park transformation, one can obtain:

$$L\begin{bmatrix} \frac{di_d}{dt} \\ \frac{di_q}{dt} \end{bmatrix} + R\begin{bmatrix} i_d \\ i_q \end{bmatrix} = u_{dc}\begin{bmatrix} S_d \\ S_q \end{bmatrix} + \begin{bmatrix} 0 & \omega L \\ -\omega L & 0 \end{bmatrix}\begin{bmatrix} i_d \\ i_q \end{bmatrix} - \begin{bmatrix} e_d \\ e_q \end{bmatrix} \tag{16}$$

$$C\frac{du_{dc}}{dt} = -\frac{3}{2}[S_d \quad S_q]\begin{bmatrix} i_d \\ i_q \end{bmatrix} - \frac{u_{dc}}{R_{Ldc}} + i_{Ldc} \tag{17}$$

3. Results and Discussions

System modeling is done as shown in Figure 2 and explained in Section 2. The DC microgrid has one 600-volt DC source, each connected to a fixed 1 kW load, while the power from the DC source will be regulated to determine the system response. In the AC microgrid, a 4 MW generator with a voltage of 400 V, a frequency of 50 Hz and a transmission with an R/X ratio of 7, is connected to the load to be regulated.

The simulation algorithm is started by setting the power source conditions in the DC microgrid as explained in Figure 5. During the simulation, two cases are considered: power changes in the DC microgrid and load changes in the AC microgrid. The simulation is carried out for 2 seconds with a schedule of power and load changes as shown in Figure 3 and Figure 4.

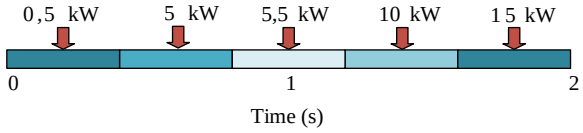

Figure 3. The schedule of power changes

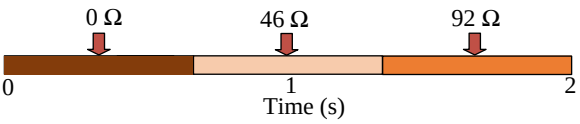

Figure 4. The schedule of load changes

In this simulation, the analysis was performed at three locations of the hybrid microgrid system: the DC microgrid, the AC microgrid, and the bidirectional converter (BC). Variations in the DC source power cause corresponding changes in the voltage and current of the DC microgrid. Figure 6 illustrates the power flow at the DC resource, the DC load, and the power transferred through the BC. When the DC power is very low or nearly zero (for example, when the PV source receives no solar irradiation), the BC transfers power from the AC microgrid to meet the DC load demand. In this condition, the power transferred through the BC becomes negative. When the DC power matches the DC load demand, the BC does not transfer power; this is indicated by the BC power value being close to zero. Conversely, when the DC power exceeds the DC load demand (i.e., when the PV operates under maximum irradiation), the BC power becomes positive, indicating that the DC microgrid is delivering excess power to the AC microgrid.

Figure 7 presents a comparison of the active power at the AC load, the grid, and the power transferred to the DC microgrid. Variations in the AC microgrid load during the simulation have minimal influence on the power transferred to the DC microgrid. The transferred power becomes negative when the grid supplies power to the system, while a positive grid power value indicates that the grid is receiving power from the DC microgrid. The power conditions within the AC microgrid corresponding to these operating states are summarized in Table 1.

The impact of power variations on the DC source can be observed not only within the DC microgrid but also in the AC microgrid. Based on the DC power changes and the AC load variations shown in Figure 3 and Figure 4, the bidirectional converter operates alternately as a rectifier or an inverter, depending on the system conditions. Despite these fluctuations in power and load, the voltage in the AC microgrid remains stable and is properly maintained throughout the simulation.

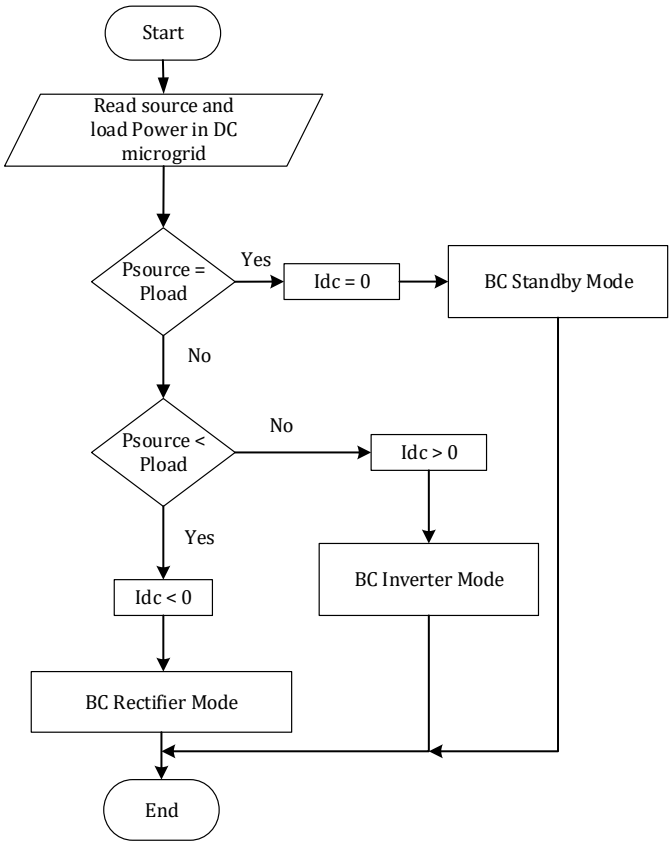

Figure 5. Simulation Algorithm

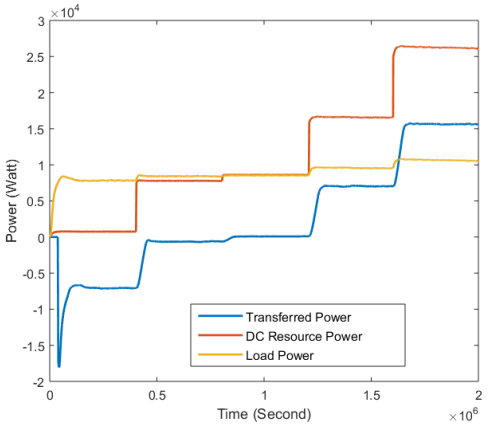

Figure 6. DC microgrid power

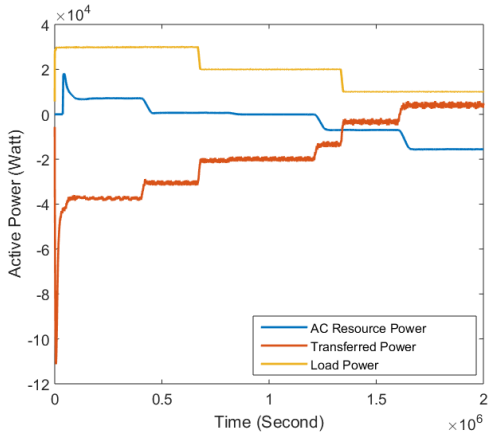

Figure 7. AC sub microgrid active power

Table 2 presents the efficiency of the converter operating in both rectifier and inverter modes. The results demonstrate that the converter can operate with very high efficiency under most conditions. However, it still encounters challenges in maintaining consistent performance when the AC and DC microgrid power levels are similar, particularly when the power transfer approaches zero. This limitation is evident from the relatively low efficiency of 65,95% at a DC microgrid power of 5kW, compared to the significantly higher efficiency of 99.62% achieved at 15 kW. This issue has not been addressed in previous studies and should be considered an important topic for future research.

Table 1. AC microgrid power

DC Power (W)	Measurement Point	Active Power / P (W)	Reactive Power / Q (VAR)
0,5 10^3	Source	-18290	-1307
	Load	10050	$1{,}33.10^{-9}$
	Line	8243	1307
	Transfer	6640	7856
5 10^3	Source	-10340	-997,4
	Load	9915	$-7{,}63.10^{-9}$
	Line	423,6	997,4
	Transfer	-34,63	2544
5,5 10^3	Source	-9632	-615,7
	Load	9917	$7{,}839.10^{-9}$
	Line	-285,3	615,7
	Transfer	-596	1639
10 10^3	Source	-3492	-348,7
	Load	9968	$-1{,}68.10^{-8}$
	Line	-6476	348,7
	Transfer	-8984	-3147
15 10^3	Source	3991	1140
	Load	10020	-4668.10^{-9}
	Line	-14010	-1104
	Transfer	-18560	-10370

Table 2. Efficiency of bidirectional converter (BC)

DC Power (W)	BC interface power (W)		Efficiency	BC Mode
	AC	DC		
0,5 10^3	6640	-6600	99,39 %	Rectifier
5 10^3	-34,63	52,51	65,95 %	Rectifier
5,5 10^3	-596	612,9	97,24 %	Inverter
10 10^3	-8984	9024	99,55 %	Inverter
15 10^3	-18560	18630	99,62 %	Inverter

A different behavior is observed in the current waveform: the AC microgrid current changes not only in magnitude but also in its phase angle relative to the voltage. In the initial condition shown in Figure 7, both voltage and current remain stable because no power or load variations have yet occurred. However, the current leads or lags the voltage, indicating that the BC is operating in rectifier mode. When the power supplied by the DC source is insufficient to meet the DC load demand, additional power is drawn from the AC microgrid. At 0.75 s, the DC power increases to a level that matches the load requirements, and the AC microgrid current reduces to nearly zero. This indicates that no current is flowing through the BC. At this moment, the BC is not functioning as either a rectifier or an inverter. Despite this, a phase shift of approximately 90° between the voltage and current is still observed.

Up to 1.25 s, the power generated in the DC microgrid increases and eventually exceeds the DC load demand. The excess power flows through the BC toward the AC microgrid, causing the phase shift between current and voltage to approach 180°, indicating that the BC has transitioned to inverter mode. At 1.6 s, the DC power increases again. Since the DC load is already fully supplied, the additional surplus power continues to be delivered to the AC microgrid through the BC. This change affects the magnitude of the current but does not alter the BC's operating mode; it remains functioning as an inverter.

The system variations that occur during the simulation also influence the harmonic content, as illustrated in Figure 8 through 11. The total harmonic distortion (THD) values closely follow the power fluctuations in the DC microgrid, rather than the load variations in the AC microgrid. Figure 8 presents the THD of the voltage measured at the output of the bidirectional converter (BC), while Figure 9 shows the THD after the voltage has been filtered by the LCL filter.

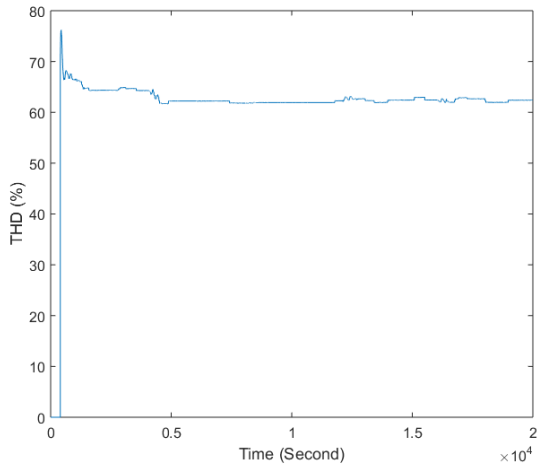

Figure 8. THD voltage in bidirectional converter side

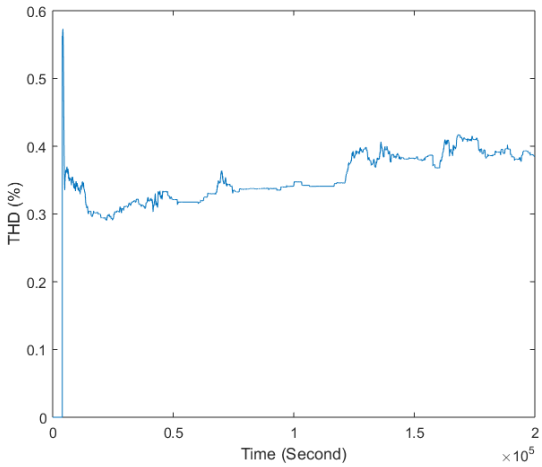

Figure 9. THD voltage in AC microgrid side

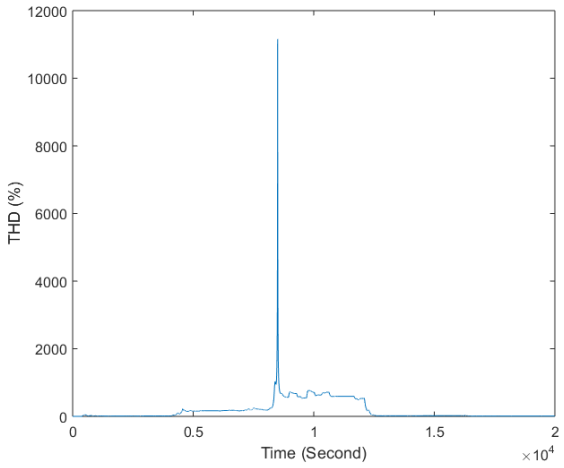

Figure 10. THD current in bidirectional converter side

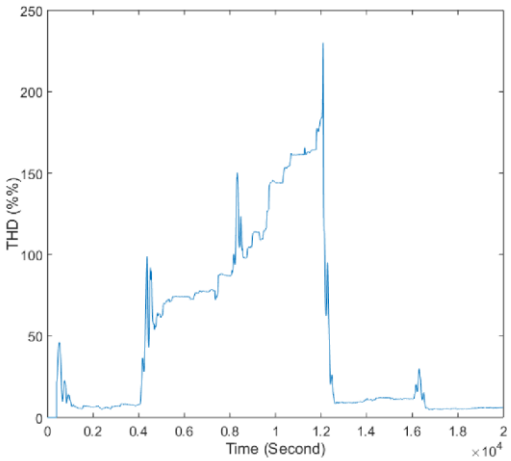

Figure 11. THD current in AC microgrid side

Figure 10 presents the THD of the current measured at the output of the BC. The figure shows that the current THD increases significantly during periods of power imbalance. Specifically, between 0.4 s and 1.25 s, the power generated by the DC source is only sufficient to supply the DC load, causing the BC to operate in neither rectifier nor inverter mode. This operating condition results in substantial harmonic distortion that exceeds the allowable limits. Even after compensation by the LCL filter, the harmonic content during this interval remains high, as illustrated in Figure 11. This is a logical event because the fundamental current flowing at that time is close to zero, where this current is a divider of the total current of other orders, this causes a drastic increase in the overall THD value. Outside of this period, the THD values return to acceptable levels and comply with the required standards.

For further research, real-time testing of this system in more complex environments, such as adding more load models and renewable energy conditions, will bring the system closer to real-world conditions. Furthermore, research combining bidirectional ac-dc control with artificial intelligence (AI) instruments, as has been done by several researchers [27], [28], will make the system more efficient in terms of overall system performance.

4. Conclusion

In this paper, a hybrid AC–DC microgrid system was developed using a bidirectional converter (BC) capable of operating in both rectifier and inverter modes. The system performed effectively, with the BC responding appropriately to power fluctuations within the DC microgrid—whether due to an increase or decrease in available power. Throughout these variations, the voltage in the AC microgrid remained stable, the THD stayed below 5%, and the system frequency was well maintained.

Load variations in the AC microgrid did not significantly influence the power transferred through the BC; however, they did affect the power drawn from or supplied to the AC grid. Although the LCL filter provides strong harmonic attenuation under steady operating conditions, its performance is compromised during transitions in the BC's operating mode (from rectifier to inverter and vice versa, standby mode). During these transitions, resonance effects can occur within the LCL filter, preventing effective harmonic damping and temporarily increasing the system's THD.

Acknowledgement

The author gratefully acknowledges the financial support from the Directorate of Research and Community Service, Ministry of Higher Education, Science, and Technology of the Republic of Indonesia.

References

[1] H. Afianti, O. Penangsang, and A. Soeprijanto, "High Performance of Power Transfer in Hybrid Ac-Dc Microgrid Without Storage System," *Journal of Engineering Science and Technology*, vol. 17, no. 1, pp. 452–471, 2022.

[2] S. H. Park, J. Y. Choi, and D. J. Won, "Cooperative control between the distributed energy resources in AC/DC hybrid microgrid," *2014 IEEE PES Innovative Smart Grid Technologies Conference, ISGT 2014*, 2014, doi: 10.1109/ISGT.2014.6816448.

[3] N. Eghtedarpour and E. Farjah, "Power control and management in a Hybrid AC/DC microgrid," *IEEE Transactions on Smart Grid*, vol. 5, no. 3, pp. 1494–1505, 2014, doi: 10.1109/TSG.2013.2294275.

[4] X. Liu, P. Wang, and P. C. Loh, "A hybrid AC/DC micro-grid," *2010 9th International Power and Energy Conference, IPEC 2010*, pp. 746–751, 2010, doi: 10.1109/IPECON.2010.5697024.

[5] B. Long, T. W. Jeong, J. D. Lee, Y. C. Jung, and K. T. Chong, "Energy Management of a Hybrid AC–DC Micro-Grid Based on a Battery Testing System," *Energies 2015, Vol. 8, Pages 1181-1194*, vol. 8, no. 2, pp. 1181–1194, 2015, doi: 10.3390/EN8021181.

[6] H. Afianti, O. Penangsang, and A. Soeprijanto, "Management strategy of hybrid microgrid to reduce multiple conversion," in *International Conference on Electrical Engineering, Informatics and Its Education 2015 (CEIE- 2015), Malang, Indonesia*, 2015, pp. 31–34.

[7] D. Yamegueu, Y. Azoumah, X. Py, and N. Zongo, "Experimental study of electricity generation by Solar PV/diesel hybrid systems without battery storage for off-grid areas," *Renewable Energy*, vol. 36, no. 6, pp. 1780–1787, 2011, doi: 10.1016/J.RENENE.2010.11.011.

[8] D. Yamegueu, Y. Azoumah, X. Py, and H. Kottin, "Experimental analysis of a solar PV/diesel hybrid system without storage: Focus on its dynamic behavior," *International Journal of Electrical Power & Energy Systems*, vol. 44, no. 1, pp. 267–274, 2013, doi: 10.1016/J.IJEPES.2012.07.027.

[9] V. Tomar and G. N. Tiwari, "Techno-economic evaluation of grid connected PV system for households with feed in tariff and time of day tariff regulation in New Delhi – A sustainable approach," *Renewable and Sustainable Energy Reviews*, vol. 70, pp. 822–835, 2017, doi: 10.1016/J.RSER.2016.11.263.

[10] Y. Azoumah, D. Yamegueu, P. Ginies, Y. Coulibaly, and P. Girard, "Sustainable electricity generation for rural and peri-urban populations of sub-Saharan Africa: The 'flexy-energy' concept," *Energy Policy*, vol. 39, no. 1, pp. 131–141, 2011, doi: 10.1016/J.ENPOL.2010.09.021.

[11] D. Tsuanyo, Y. Azoumah, D. Aussel, and P. Neveu, "Modeling and optimization of batteryless hybrid PV (photovoltaic)/Diesel systems for off-grid applications," *Energy*, vol. 86, pp. 152–163, 2015, doi: 10.1016/J.ENERGY.2015.03.128.

[12] M. Liserre, F. Blaabjerg, and S. Hansen, "Design and control of an LCL-filter-based three-phase active rectifier," *IEEE Transactions on Industry Applications*, vol. 41, no. 5, pp. 1281–1291, 2005, doi: 10.1109/TIA.2005.853373.

[13] M. Liserre, A. Dell'Aquila, and F. Blaabjerg, "Stability improvements of an LCL-filter based three-phase active rectifier," *PESC Record - IEEE Annual Power Electronics Specialists Conference*, vol. 3, pp. 1195–1201, 2002, doi: 10.1109/PSEC.2002.1022338.

[14] D. Solatialkaran, F. Zare, T. K. Saha, and R. Sharma, "A Novel Approach in Filter Design for Grid-Connected Inverters Used in Renewable Energy Systems," *IEEE Transactions on Sustainable Energy*, vol. 11, no. 1, pp. 154–164, 2020, doi: 10.1109/TSTE.2018.2887079.

[15] M. Dursun and M. K. Dosoglu, "LCL Filter Design for Grid Connected Three-Phase Inverter," *ISMSIT 2018 - 2nd International Symposium on Multidisciplinary Studies and Innovative Technologies, Proceedings*, 2018, doi: 10.1109/ISMSIT.2018.8567054.

[16] A. Kouchaki and M. Nymand, "Analytical Design of Passive LCL Filter for Three-Phase Two-Level Power Factor Correction Rectifiers," *IEEE Transactions on Power Electronics*, vol. 33, no. 4, pp. 3012–3022, 2018, doi: 10.1109/TPEL.2017.2705288.

[17] H. Alrajhi, S. A. Raza, H. Babsail, and A. Alattas, "Design, analysis and comprehensive assessment of LCL filters for VSC applications," *Journal of Umm Al-Qura University for Engineering and Architecture*, vol. 16, no. 3, pp. 559–573, 2025, doi: 10.1007/S43995-025-00132-1/TABLES/5.

[18] A. Bouledroua, T. Mesbah, and S. Kelaiaia, "Artificial neural network maximum power point tracking for mitigation photovoltaic harmonic distortion," *Bulletin of Electrical Engineering and Informatics*, vol. 14, no. 6, pp. 4161–4173, 2025, doi: 10.11591/EEI.V14I6.10050.

[19] A. ; Tian *et al.*, "Harmonic Self-Compensation Control for Bidirectional Grid Tied Inverter Based on Crown Porcupine Optimization Algorithm," *Electronics 2024, Vol. 13, Page 2607*, vol. 13, no. 13, p. 2607, 2024, doi: 10.3390/ELECTRONICS13132607.

[20] J. Huang, J. Xiao, C. Wen, P. Wang, and A. Zhang, "Implementation of Bidirectional Resonant DC Transformer in Hybrid AC/DC Micro-Grid," *IEEE Transactions on Smart Grid*, vol. 10, no. 2, pp. 1532–1542, 2019, doi: 10.1109/TSG.2017.2771822.

[21] H. Afianti, O. Penangsang, and A. Soeprijanto, "Stability and reliability of low voltage hybrid AC-DC microgrids power flow model in islanding operation," *Indonesian Journal of Electrical Engineering and Computer Science*, vol. 19, no. 1, pp. 32–41, 2020, doi: 10.11591/IJEECS.V19.I1.PP32-41.

[22] G. Wang, X. Wang, and J. Lv, "An Improved Harmonic Suppression Control Strategy for the Hybrid Microgrid Bidirectional AC/DC Converter," *IEEE Access*, vol. 8, pp. 220422–220436, 2020, doi: 10.1109/ACCESS.2020.3042572.

[23] A. Reznik, M. G. Simoes, A. Al-Durra, and S. M. Muyeen, "LCL Filter design and performance analysis for grid-interconnected systems," *IEEE Transactions on Industry Applications*, vol. 50, no. 2, pp. 1225–1232, 2014, doi: 10.1109/TIA.2013.2274612.

[24] A. Mohamed, S. R. B. Vanteddu, and O. Mohammed, "Protection of bi-directional AC-DC/DC-AC converter in hybrid AC/DC microgrids," *Conference Proceedings - IEEE SOUTHEASTCON*, 2012, doi: 10.1109/SECON.2012.6196958.

[25] A. Mohamed, M. Elshaer, and O. Mohammed, "Bi-directional AC-DC/DC-AC converter for power sharing of hybrid AC/DC systems," *IEEE Power and Energy Society General Meeting*, 2011, doi: 10.1109/PES.2011.6039868.

[26] X. Zheng, F. Gao, H. Ali, and H. Liu, "A Droop Control Based Three Phase Bidirectional AC-DC Converter for More Electric Aircraft Applications," *Energies 2017, Vol. 10, Page 400*, vol. 10, no. 3, p. 400, 2017, doi: 10.3390/EN10030400.

[27] S. Rajendran, V. Thangavel, N. Krishnan, and N. Prabaharan, "DC Link Voltage Enhancement in DC Microgrid Using PV Based High Gain Converter with Cascaded Fuzzy Logic Controller," *Energies 2023, Vol. 16, Page 3928*, vol. 16, no. 9, p. 3928, 2023, doi: 10.3390/EN16093928.

[28] P. Yanna, R. & Lalit, C. Saikia, P. Y. Reddy, and L. C. Saikia, "Hybrid AC/DC control techniques with improved harmonic conditions using DBN based fuzzy controller and compensator modules," *Systems Science & Control Engineering*, vol. 11, no. 1, p. 2188406, 2023, doi: 10.1080/21642583.2023.2188406.